Magnetotransport and flux pinning characteristics in $R\mathrm{Ba_2Cu_3O_{7-\delta}}$ ($R=\mathrm{Gd,Eu,Nd}$) and $(\mathrm{Gd_{1/3}Eu_{1/3}Nd_{1/3}})\mathrm{Ba_2Cu_3O_{7-\delta}}$ high-T_c superconducting thin films on SrTiO₃(100)

C. Cai, B. Holzapfel, J. Hänisch, L. Fernández, and L. Schultz

Leibniz Institute for Solid State and Materials Research (IFW), Helmholtz strasse 20, 01069 Dresden, Germany

High-quality mono rare earth $R\mathrm{Ba_2Cu_3O_{7-\delta}}$ ($R=\mathrm{Gd,Eu,Nd}$) and mixed rare earth $(\mathrm{Gd_{1/3}Eu_{1/3}Nd_{1/3}})\mathrm{Ba_2Cu_3O_{7-\delta}}$ (GEN123) films were prepared by off-axis laser deposition, and their transport and flux pinning characteristics were experimentally studied. Enhanced flux pinning due to rare earth mixing is evidenced by high transport critical current density (J_c) and an upward shifted irreversibility line defined by zero-resistance criterion. In contrast, the characteristic field, i.e. the accommodation field (H_{acc}), identified from the field dependence of transport J_c, shows no increase due to rare earth mixing. It is found that H_{acc} vs T can be scaled by a negative exponential relation at a wide range of temperatures, and the field anisotropy of H_{acc} appears pronounced as the field direction varies from $H\|c$ to $H\|(a,b)$. According to the analysis on the temperature dependence of J_c, it is suggested that the flux pinning mechanism in mixed rare earth samples is dominated by stress-field centers which may be induced by dislocations and enhanced by lattice mismatch in GEN123 films. Finally, the fluctuation of vortex phases is discussed with respect to correlated and uncorrelated structure disorders in epitaxial 123 thin films.

I. INTRODUCTION

It is well known that the critical current density J_c in epitaxial high-temperature superconducting $R\mathrm{Ba_2Cu_3O_{7-\delta}}$ (R123) films is typically two orders of magnitude higher than in twinned single crystals and melt-textured bulks. The origin and mechanism of flux pinning in epitaxial R123 films have been extensively studied,[1–6] but still remain unclear. Initial research suggested several possible types of effective pinning source in R123 films, including low-angle grain boundaries, precipitates, twins, surface roughness, screw dislocations etc.[1,2,7,8] Recently, most attempts have been to establish a correlation between strong pinning roles with columnar defects induced by irradiation, screw dislocations corresponding to three-dimensional growth, and growth steps on the surface associated with two-dimensional layer-by-layer growth.[3–6] Dam *et al.*[3] quantitatively mapped both the edge and screw dislocations by a sequential etching technique, and indicated that these dislocations are the linear defects that provide the strong pinning centers responsible for the high critical currents in thin films. However, Pan *et al.*[7] argued that the screw and edge dislocations themselves can hardly be effective pinning centers as their characteristic transverse sizes are much greater than the coherence length. They proposed that the dislocation lines (i.e. the cores of dislocations) may act as exceedingly strong one-dimensional linear pinning centers as these cores, formed during the film deposition and growth, resemble those of artificial defects introduced by irradiation with heavy ions of high energy. Moreover, Fedotov *et al.*[8] noted that low-angle grain boundaries (GBs) between single-crystal blocks or so-called growth islands separated by trenches are characteristic structures for epitaxial films obtained by various deposition techniques, and thus they stress that the GB network representing a quasiperiodic chain of edge dislocations governs the effective flux pinning. In spite of the above arguments, it

is generally accepted that as-grown linear defects (either dislocations, dislocation lines, or the GB network) nucleate at or correlate with the growth islands separated by trenches, or their substructures. Aside from these linear defects, randomly distributed pointlike disorders such as oxygen vacancies and stress-field centers, as discussed in this paper, are also appreciable pinning sources contributing to a high critical current density.[9,10]

Flux pinning mechanisms are mainly classified into two types:[11,12] (i) δT_c due to the spatial fluctuation of the Ginsburg-Landau coefficient associated with the transition temperature T_c, and (ii) δl induced by the spatial fluctuation of the effective mass related to the charge carrier mean free path l. Griessen *et al.*[12] demonstrate that pinning in pure Y123 thin films is mainly of δl type, whereas Wen *et al.*[13] found evidence of δT_c in single domain (Y, Pr)123. Furthermore, they demonstrated the existence of extra pinning centers in Gd-substituted Y123 thin films.[9] Using the generalized inversion scheme, they also developed a theoretical expression for $J_c(T)$ and the pinning potential $U_c(T)$ with respect to the stress field in the substituted film.

Pinning enhancement due to chemical substitution or addition of second phases is frequently reported for melt-textured R123 bulks.[14–17] Although only few authors establish the dominating pinning mechanism in such a complicated system, it is obvious that optimum composition fluctuation is an effective method for improving the critical current density. Recently, Muralidhar and co-workers[16,17] did a series of works on the effect of mixed light rare earths in R123 melt-textured bulks. They achieved a high J_c of 7 $\times 10^4$ A/cm² at the field of 4.5 T, and an extraordinary irreversibility field of 15 T at 77 K.[16] There has, however, been no effort to study the effect of rare earth mixing in thin film systems. In the present work, we report high-quality mixed rare earth 123 thin films where three isovalent light rare earths, Gd, Eu, and Nd are incoporated in equal atomic

amounts. The constituent $R123$ has a similar T_c, while the lattice parameter differs to some extent. It is imaginable that rare earth mixing will increase imperfection or composition fluctuation but does not change T_c very much. This differs from the case of the partial substitution of R with divalent Ca which results in pronounced depression of T_c. Note that the chemical route to modify flux pinning in thin films is interesting not only for fundamental understanding but also for practical applications, particularly for coated conductors emerged with epitaxial film growth techniques. In the past few years, people paid main attention to weak linking at grain boundaries for the achievement of high J_c in coated conductors. However, it was recently found that the J_c at high fields is mainly limited by the properties of intragrains, rather than of grain boundaries.[18] Hence, it should be emphasized that improving the flux pinning is essentially significant for high J_c and high field applications of coated conductors. In the following sections, we will give experimental details for the thin film growth, transport critical current density and its field and temperature dependences, and then discuss flux pinning characteristics in the rare earth mixed 123 films.

II. EXPERIMENTAL DETAILS

A. Growth of GEN123 thin films

Off-axis laser ablation technique[19] was used to prepare a series of mono and mixed rare earth 123-type superconducting thin films. Substrates are single crystals of (100) $SrTiO_3$. Ternary and mono rare earth $R123$ ($R=$ Gd, Eu, or Nd) targets were prepared with the stoichiometric compounds sintered and ground in three cycles from mixed powders of R_2O_3, $CaCO_3$, and CuO. The resultant targets, checked by x-ray diffraction and inductive T_c measurement, are of pure 123 phases comprising the nominal compositions: $(Gd_{1/3}Eu_{1/3}Nd_{1/3})Ba_2Cu_3O_y$, $GdBa_2Cu_3O_{7-\delta}$, $NdBa_2Cu_3O_{7-\delta}$, and $EuBa_2Cu_3O_{7-\delta}$.

A KrF excimer laser with a wavelength of 248 nm (Lambda Physik LPX305) was used at a fixed repetition of 5 Hz and an energy density of ~ 3 J/cm^2 on the target surface. Deposition temperatures (T_s) varying from 650 to 850 °C, and an oxygen partial pressure $p(O_2)$ in the range of 0.15–0.30 mbar were used. Oxygen annealing was performed in situ with pure oxygen of 700 mbar at temperatures of 300–400 °C for 30 min, followed by slowly cooling down to room temperature. The deposition rate reached 0.1–0.3 Å/pulse, generally lower than that of on-axis geometry which is typically around 1 Å/pulse. The temperatures given above and below are the heater temperatures, whereas the sample surface temperature, measured using a pyrometer, can be up to 50 °C higher depending on oxygen pressure.

It is found that unlike mono rare earth $R123$ or Y123, optimum growth of GEN123 is limited to a narrow range of $p(O_2)$ and T_s. Moreover, the lower in-situ oxygenating temperature (T_a) (compared with Y123) is favorable for the achievement of high T_c and small δT_c, implying a different orthorhombic-tetragonal phase transition temperature from Y123, which may be associated with the distinct oxygen-
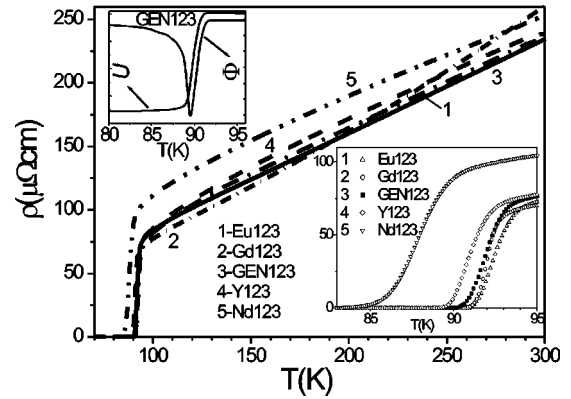

FIG. 1. Resistivity-temperature transitions for GEN123 and $R123$ thin films. The top left inset shows an inductive T_c measurement on unpatterned GEN123 (U for inductive voltage, and Φ for phase, both in arbitrary units). The bottom right inset is an enlargement of the main plot.

ordering superstructure occurring in the $R123$ with a R ionic radius larger than Y.[20] By means of optimized conditions: $p(O_2) \sim 0.22$ mbar, $T_s \sim 780$ °C, and $T_a \sim 310$ °C, we achieved high quality GEN123 thin films with $T_c = 90.2$ K and $\delta T_c \sim 2$ K as shown in Fig. 1. Note that the given T_c is measured on unpatterned samples using an inductive setup. Its value is determined by 90% increase in induced voltage at the warming-up stage, which corresponds to the zero resistance $T_c(R=0)$ in transport measurement where percolation effects usually make the transition width narrower. The above process conditions are also able to produce Gd123 and Eu123 of high quality ($T_c = 91$ K and $\delta T_c \sim 1.5$ K), although Nd123 has a broadened δT_c (~ 4–8 K). All the present samples were prepared with the same processing conditions mentioned above and have a similar thickness of around 50 nm.

B. Grain orientation and surface morphology

The crystal structure was examined using a four-circle diffractometer. The c-axis orientation and in-plane texture were identified for all the present films by observing the (001) peaks in θ-2θ diffraction and full width at half maximum (FWHM) of four symmetric peaks in the (103) pole figure. Figure 2 shows a typical θ-2θ pattern for a GEN123 film and the referenced Gd123 film. Apart from substrate peaks, only (00l) peaks from 123 phases completely overlapping between GEN123 and Gd123 reveals that rare earth mixing does not give rise to extra phases or a deviation from c-axis orientation. The out-of-plane textures are as good as FWHM $\sim 0.6°$ for the (005) rocking curve. Phi scanning of a (103) peak gives FWHM $< 2°$, indicating a good in-plane texture as well.

Surface morphology and microstructure were observed using scanning electron microscopy (SEM, JEOL-6400) and atomic force microscopy (AFM, Digital Instruments Nanoscope III). As shown in Fig. 3(a), typical GEN123 films appear smooth and uniform in SEM images. Almost no droplets or pinholes are evident. This can be attributed to the employment of the off-axis deposition technique which has
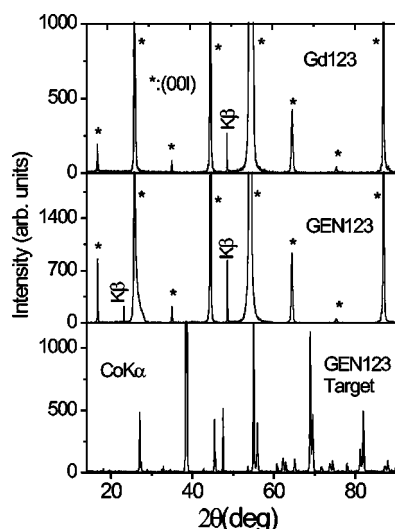
FIG. 2. Typical x-ray diffraction patterns for GEN123 and Gd123 thin films. The c-axis orientation is evidenced by $(00l)$ reflections($*$). The diffraction pattern of the polycrystalline GEN123 target is also shown.

proven effective in eliminating droplets and improving the homogeneity of composition.[19,21] In contrast, the films show a regularly spaced array of growth islands under AFM observation [see Fig. 3(b)]. These islands are partially separated by trenches with depths of 5–15 nm, and connected at the base or merging with each other at a certain height. The island density and average dimension are around 40 per μm^2 and 130 nm in diameter, respectively. To acquire more defect-related information, the films were softly etched in an iodine or bromine/ethanol solution for 5–30 min. Figure 3(c) shows a typical image for both the etched GEN123 and R123 films. It is characterized by two-dimensional nucleation and terraced growth traces, while spiral growth appears in only a few of the islands. Within the growth island, concentric growth steps with large and flat areas of 100–150 nm are frequently observed. The step heights vary between 1 and 5 nm (1–4 unit cells). The step spacing is between 10–20 nm. In general, there is no obvious difference in the above features between GEN123 and pure R123 films. This may be due to the same processing conditions and thickness, and a similar growth mode insensitive to rare earth mixing.

C. Electrical transport measurements

Resistivity and current-voltage curves at various temperatures and magnetic fields were measured using a Quantum Design PPMS. A standard four-contact method was used in a bridge geometry patterned by photolithography. The zero resistance point and critical current density were determined using an electrical field criterion of 1 μV/cm. In the present measurements, the field was applied perpendicular to the current direction, and parallel to the c axis, except where stated otherwise. Figure 4(a) shows the resistance-temperature (R-T) transitions in various magnetic fields. Zero-field R-T transitions for typical R123 and GEN123 films show a similar residual resistivity ratio [RRR = $R(300$ K)/$R(95$ K)] of
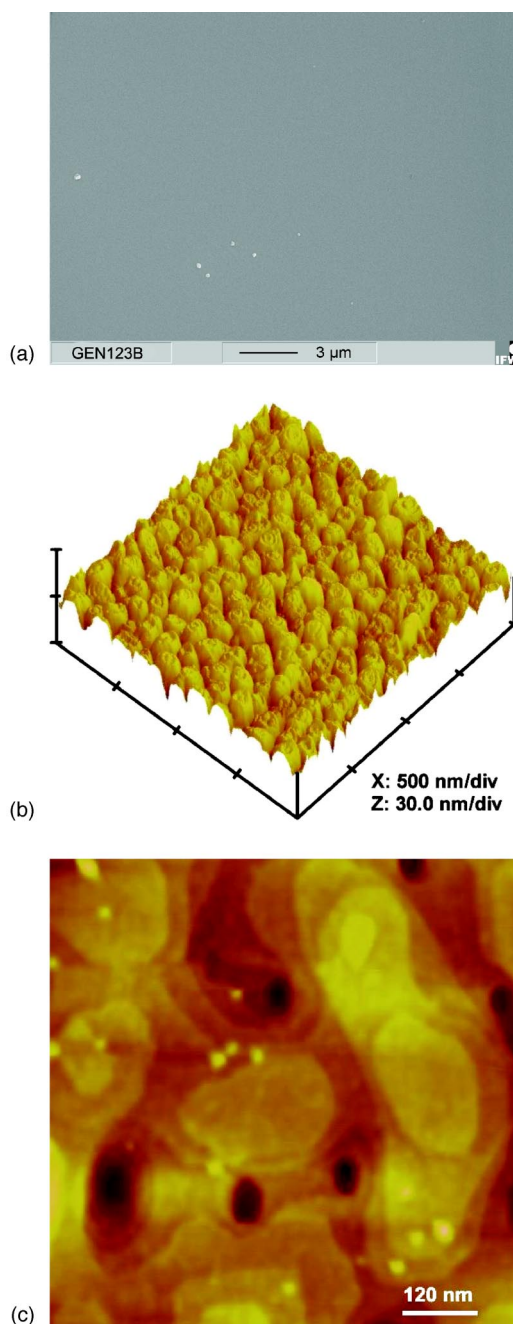

FIG. 3. (Color online) (a) SEM images of GEN123 showing a smooth and droplet-free surface morphology. (b) Growth island characteristics under AFM observation. (c) AFM images for softly etched GEN123 characterized by terraced growth with concentric flat.

3.0–3.7 (see Fig. 1). Gd123 has the highest RRR and narrowest δT_c. For comparison, Gd123 was selected as the reference sample in the following study on GEN123. Figure 4 shows a series of isothermal I-V curves. These were either measured with field variation at a fixed temperature [Fig. 4(b)], or with temperature variation at a fixed applied field [Fig. 4(c)], both of which are plotted in double logarithmic scale.
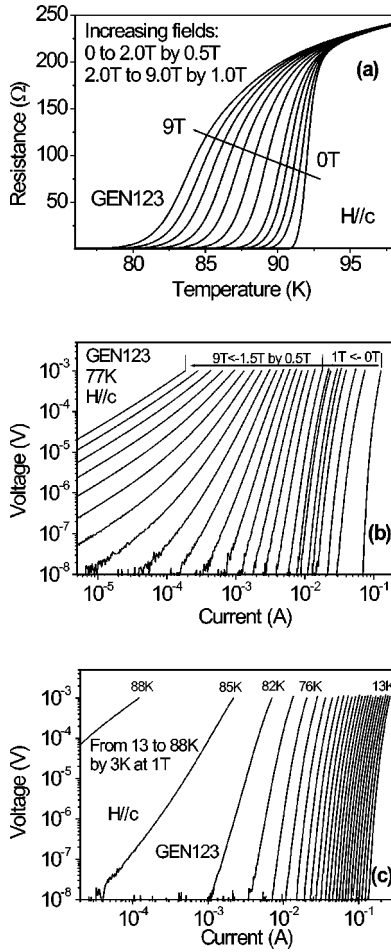
FIG. 4. Magnetotransport measurements for patterned GEN123 thin films: (a) Resistance-temperature curves in various magnetic fields. (b) Double logarithmic plots of voltage vs current at 77 K in various magnetic fields. (c) Double logarithmic plots of voltage vs current at 1 T for various temperatures.

III. RESULTS AND DISCUSSION

A. Irreversibility line

The irreversibility line (hereafter referred to as the IRL) is one of the distinguished features of high-temperature super-conductors. The IRL is far away from $H_{c2}(T)$, the upper critical field described by mean-field theory. It divides the H-T plane into two major regions: below the IRL, a non-equilibrium distribution of flux line owing to the pinning effects, and above the IRL, an equilibrium state due to strong flux motion.[11,22] The irreversibility lines were determined from the R-T measurements with the criterion of zero resistance and are shown in Fig. 5. They represent the flux dynamic characteristic in the films, essentially displaying the change from the regime dominated by flux pinning to one dominated by thermally activated flux flow where dissipative resistance appears. For each GEN123 and R123 film, the IRL is well fitted with a power law of $H_{irr} \propto \alpha (1 - T/T_c)^{\beta}$. The exponent β is 1.526 $(H\|c)$ and 1.450 $[H\|(a,b)]$ for GEN123, and 1.335 $(H\|c)$ and 1.28 $[H\|(a,b)]$ for Gd123. These values are in agreement with the experimental results of other authors $(\beta \sim 1.33$–$1.50)$,[11,23] while remaining lower
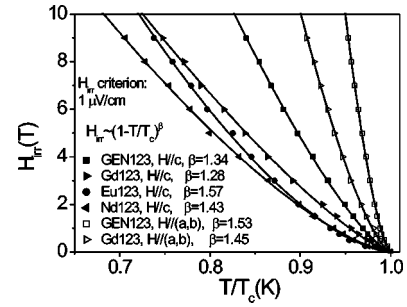

FIG. 5. Irreversibility lines for GEN123 and R123 determined by zero resistance. Solid lines are a fit to $H_{irr} \propto (1 - T/T_c)^{\beta}$.

than that $(\beta \sim 2)$ predicted by the melting theory.[23] Clearly, GEN123 shows a higher exponent than pure R123 films. Accordingly, IRL shifts to higher temperatures and fields, not only for $H\|c$, but also for $H\|(a,b)$ where intrinsic pinning is involved.

B. Critical current density

The improved irreversibility behavior implies the enhancement of flux pinning and associated J_c. Indeed, it was found that J_c in the mixed rare earth films reaches 3.7 MA/cm^2 at 77 K and in a self-field, approximately three times higher than in the pure R123 films including Y123. Figure 6(a) shows the temperature dependence of J_c with and without applied field. Compared with the referenced Gd123, GEN123 has an improved J_c at all temperatures, being more enhanced at high temperatures. This implies that the effect of rare earth mixing on flux pinning is more pronounced when the vortex state approaches the IRL where thermally activated flux motion will take place. In addition,
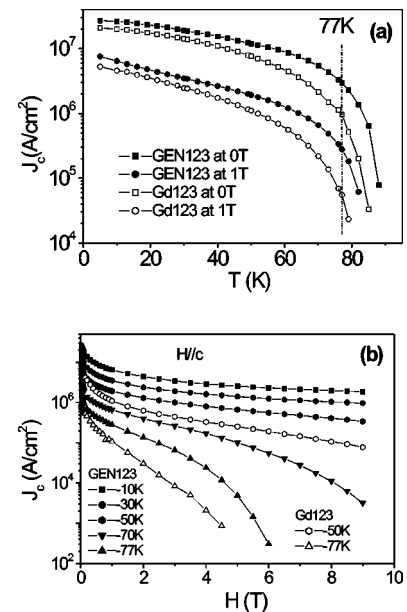

FIG. 6. Improved J_c of GEN123 in comparison with that of Gd123. (a) Temperature dependence of J_c with and without applied fields. (b) Field dependence of J_c at temperatures of 5, 30, 50, 77, and 85 K.
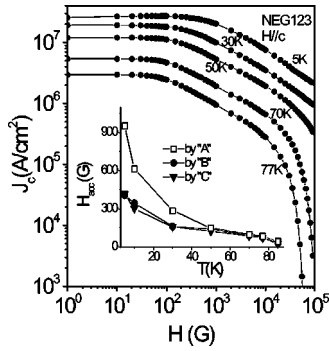
FIG. 7. Field dependence of J_c on a log-log scale [Fig. 6(b) replotted]. The inset shows the temperature dependence of the accommodation field H_{acc} determined by three different methods: by the crossing of the low-field plateau with a power fit (A) or with a logarithmic fit (B) at the intermediate fields, or by a criterion of reduction in J_c such as 90% (C).

$\log J_c$ drops linearly with T at the low-temperature region for both GEN123 and Gd123, in agreement with the prediction of the collective-pinning theory.[11,24,25] The temperature dependence of J_c will be further analyzed in Sec. III D.

Figure 6(b) shows the dependence of J_c on applied magnetic fields between 0 and 9 T at several temperatures, which also demonstrate the enhancement of J_c in GEN123. Note that off-axis deposited R123 thin films usually show a relatively low transport J_c,[19] typically 1 MA/cm^2, in comparison with 2–3 MA/cm^2 in ideal on-axis samples. A possible reason for this is the smooth morphology and homogenous composition leading to a decrease in defect density for off-axis samples. We assume that the J_c values attainable for both GEN123 and Gd123 could be higher in the case of on-axis deposition.

C. Field dependence of J_c and accommodation field

To see further features of the field dependence of J_c, the curves of Fig. 6(b) are replotted in Fig. 7 on a log-log scale. The field unit is hereinafter changed into Gauss for the convenience to addressing low field characteristics. It is apparent that the field dependence of J_c is divided into two or three regimes. In the low field regime, J_c is nearly independent of the applied field indicated by a plateau. In the intermediate regime, J_c decreases by a power law, and then drops sharply at high fields. The third regime is either evident or not depending on the proximity of the IRL to the experimental temperatures and fields. A characteristic field is established from the crossover at the first kink of $J_c(H)$ as described in numerous oxide superconductors with correlated disorders such as columnar defects introduced by heavy ion irradiation.[3,5] In the theoretical H-T phase diagram, this characteristic field is termed the accommodation field[5–7] H_{acc}, marking the crossover from strong individual pinning to weak collective pinning. It has also been called the "interaction field," below which vortex-vortex interactions are negligible and J_c is expected to be field independent.[6] Experimentally, one may determine H_{acc} in three ways: by the intersection of the low-field plateau and a power law fit to
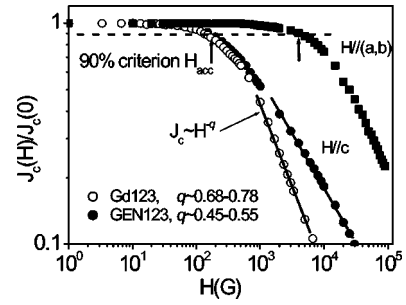

FIG. 8. A comparison of H_{acc} and the slope of the linear segment at intermediate $\log J_c$–$\log H$ plot between GEN123 and Gd123. The field anisotropy of H_{acc} is evidenced as well.

the intermediate field regime;[5] by the intersection of the low-field plateau and a logarithmic fit at the following kink to the relation $J_c(H)/J_c(0) = \gamma \ln(H_{acc}/H)$, where γ is a fitting parameter;[8] or with a criterion of J_c reduction such as $J_c(H_{acc})/J_c(0) = 0.63 \sim 0.90$.[5,26] In the case of ionirradiated Y123 single crystals, Krusin-Elbaum *et al.*[5] defined $H_{acc} \leq H_\Phi$, where H_Φ is the so-called matching field, at which the densities of defects and vortices are equal. They determined H_{acc} by the first method, i.e., by the intersection of the low-field plateau and subsequent power law: $J_c(H) \sim H^{-1}$. They also showed experimentally that this method corresponds to a criterion of $J_c(H_{acc})/J_c(0) = 0.63$. In this work, we employed a criterion of $J_c(H_{acc})/J_c(0) = 0.90$, as suggested by Mezzetti *et al.*[26] This simple method seems to be more reliable and reasonable for two reasons. First, the resulting H_{acc} is comparable with that of the second method, which is constructed according to a physical mechanism involving the depinning of the ensemble of vortices pinned at edge dislocations in the growth island network which is a characteristic for our films. Second, the H_{acc} obtained from the first method is dependent on the slope of power law at intermediate fields, rather than the logarithmic behavior which gives ideal fitting in the region of the kink. From the inset of Fig. 7, it is clearly seen that the first method results in an unreasonably large H_{acc}, especially at low temperatures.

Figure 8 shows the anisotropy of H_{acc} with respect to the direction of applied fields. H_{acc} for $H\|c$ is quite low, but pronouncedly large for $H\|(a,b)$ when intrinsic flux pinning occurs. Such a strong field anisotropy of H_{acc} in GEN123 films apparently differs from that in melt-textured Y123 bulks where the H_{acc} anisotropy is very weak or even negligible.[27] Recalling the well known fish-tail effect that is frequently reported in melt-textured R123 and rare earth mixed 123 bulks,[15,16] but never found in thin films, we suppose that there exists an essential difference in the flux pinning mechanism between thin films and bulk materials. This is a complex topic, beyond the scope of this paper.

The temperature dependence of H_{acc} is shown in Fig. 9. H_{acc} decreases exponentially with increasing temperature (at least up to 77 K), rather than linearly as concluded in Ref. 5. Also, no effects of deleterious thermal depinning reduce H_{acc} to zero at $T = 40$ K as reported for irradiated samples.[5,28]
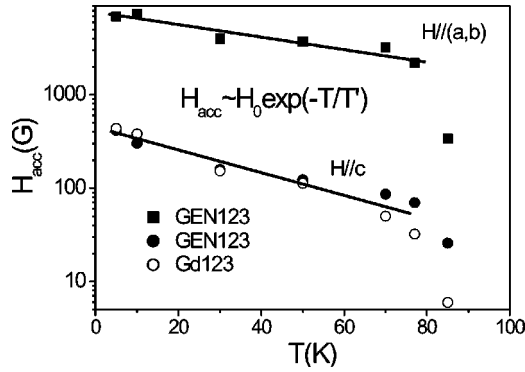
CAI, HOLZAPFEL, HÄNISCH, FERNÁNDEZ, AND SCHULTZ PHYSICAL REVIEW B **69**, 104531 (2004)

FIG. 9. Temperature dependence of H_{acc} for $H\|c$ and $H\|(a,b)$. Over a large temperature range, H_{acc} vs T scales as negative exponential decay.

For both parallel and perpendicular fields, H_{acc} vs T scales as $H_o \exp(-T/T')$, where the fitting parameters T' and H_o are ~ 65 K and 0.77 T for $H\|c$, and 440 K and 0.0038 T for $H\|(a,b)$, respectively. When the temperature approaches T_c, H_{acc} drops sharply to zero.

After comparing the extensive results in Y123, R123, and GEN123 thin films, it is apparent that H_{acc} is more subject to growth conditions, film thickness etc. than rare earth composition. As seen from Figs. 8 and 9, H_{acc} of GEN123 is not higher (even a little lower at some temperatures) than that of Gd123. This implies that rare earth mixing itself is not capable of increasing H_{acc} although such mixing clearly improves J_c as well as H_{irr}. The insensitivity of H_{acc} to rare earth mixing is understandable if one recalls that H_{acc} is mainly dependent on the pinning at linear defects which have been experimentally numbered as n_{disl}, proportional to the growth island density.[3] We suppose that our GEN123 has a comparable n_{disl}, and hence a H_{acc} close to that of Gd123 since they have similar size and density of growth islands evidenced by AFM observation. Unlike H_{acc}, J_c depends on more extended defects, particularly in the case of collective pinning with vortex-vortex interactions. The effect of rare earth mixing on J_c is not overshadowed by the role of linear defects.

Until now, we have not discussed the field dependence of J_c at intermediate fields. To fit the data in the range of $0.1 < J_c(H)/J_c(0) < 0.7$ which covers the majority of the linear regime in the $\log J_c$ vs. $\log H$ plot, we find that J_c scales as H^{-q}. The exponent q is $\sim 0.50 \pm 0.05$ for GEN123 films, in contrast to $\sim 0.73 \pm 0.05$ for Gd123 films, which present a relatively gradual slope in the log-log plot. Together with the large value of J_c, the reduced power-law decay of J_c with H is another demonstration of enhanced vortex pinning in GEN123 films.

D. Stress field induced flux pinning mechanism

Although rare earth mixing seems to be ineffective in increasing correlated linear defects, and associated H_{acc}, it could produce uncorrelated disorder, i.e., a random distribution of defects (e.g., globular nonsuperconducting regions of the size of the superconducting coherence length ξ), and thus

enhance flux pinning. Additional pinning in GEN123 may originate from stress field centers. In reality, stress fields are widely present around the defects such as dislocations found in both metallic and oxide superconductors.[29–31] In element-substituted thin films, additional stresses are created by the locally disturbed lattice, i.e., lattice misfit. Since the spatial distribution of stress field is attenuated as $1/r^6$, their influence range is rather localized, being comparable with ξ.[9,15] Pinning enhancement due to stress fields has been evaluated for Ho doped Y123 films and bulk materials,[14,15] and for Dy or Gd doped Y123 films.[9,10] We assume that stress fields induced by lattice misfit are randomly distributed in our rare earth mixed films, contributing to flux pinning in a collective behavior, leading to higher J_c, and an upwards shift of the ILR. The contribution may become more remarkable when vortex matter enters the regime of vortex-vortex interaction, i.e., at $H > H_{acc}$, resulting in the suppressed power decay of J_c with H. Note that the enhanced pinning from oxygen deficiencies can be overlooked as both the GEN123 and Gd123 films presented here are optimally doped, having similar T_cs as high as 92 K.

To further understand the stress field induced pinning mechanism, we return to analyzing the experimental temperature dependence of J_c. So far, we have not pointed out the difference between true superconducting (i.e. depairing) critical current density (J_s) and the measured J_c at a certain electric field criterion. In reality, J_c is reduced from J_s by thermal activation effects. According to the model of thermally activated flux motion and the model of collective flux pinning,[23–25] J_s and J_c follow the relation

$$J_c(T) = J_s(T) \left/ \left[1 + \frac{\mu k_B T}{U_c} \ln(t_m/t_{\text{eff}} + 1) \right]^{1/\mu} \right., \quad (1)$$

where U_c is the pinning potential, k_B is Boltzmann's constant, μ is a characteristic index of the collective pinning model, t_m is the time during which J_c data are collected, and t_{eff} is an effective attempt time for a vortex or bundle to jump over a potential barrier. In the discussion below, $J_c(T)$ and $U_c(T)$ will be written as $J_c(T) = J_c(0)f(t)$, and $U_c(T) = U_c(0)g(t)$, where $t = T/T_c$.

Blatter et al.[11] realized that all quantities characterizing the collective pinning of a single vortex can be expressed in terms of a disorder parameter. According to these expressions and the generalized inversion scheme, Griessen et al.[12] derived the temperature dependence of $f(t)$ and $g(t)$ for two main types of pinning mechanism, δT_c and δl pinning. For pure Y123 thin films, they concluded that the main pinning is of δl type. Accordingly, $f(t)$ and $g(t)$ are given as below:

$$f(t) = (1-t^2)^{7/6}(1+t^2)^{5/6}, \quad (2a)$$

$$g(t) = (1-t^2)^{1/3}. \quad (2b)$$

As previously mentioned, Wen et al.[9] developed the ideal of the pinning mechanism related to stress fields, and established a theoretical model which gives $f(t)$ and $g(t)$ as below:
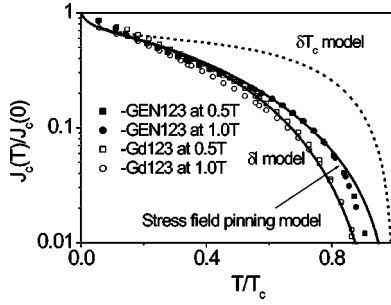
$$f(t) = (1-t^2)^{7/6}(1+t^2)^{-11/6}, \quad (3a)$$

104531-6

FIG. 10. Fitting of normalized $J_c(T)$ with various pinning models.

FIG. 11. Shifts of H-T phases due to structural disorders in epitaxial 123 thin films. The solid and dashed lines are drawn according to the fitting of $H_{irr}(T)$ and $H_{acc}(T)$ mentioned in the text.

$$g(t) = (1-t^2)^{1/3}(1+t^2)^{1/3}. \tag{3b}$$

From Eq. (1), it is easy to see that $J_c(0) = J_s(0)$ at $T = 0$ K. Thus

$$J_c(T)/J_s(0) = f(t)/[(1+\mu k_B S T_c t/g(t))]^{1/\mu}, \tag{4}$$

where $S = \ln(t_m/t_{eff}+1)/U_c(0)$. As each J_c is measured in the same time interval t_m, and $t_m \gg t_{eff}$, we can take $\ln(t_m/t_{eff}+1)$ together with $U_c(0)$ as a constant. During the experiment, if J_c is not too far from J_s, μ is 1/7 as suggested by Feigel'man *et al.*[25] Consequently, it is feasible to fit our experimental $J_c(T)$ by Eq. (4) with only one unknown parameter S. As shown in Fig. 10, normalized $J_c(T)$ for GEN123 are well fitted over the main temperature range with the model of stress field pinning, while Gd123 films agree with the model of δl. When the temperature approaches the irreversibility temperature, the increased thermally activated flux flow requires stronger pinning resulting in the stress field no longer dominating. As a result, $J_c(T)$ tends to follow the underlying mechanism of δl pinning until the quenching of the superconducting current at the irreversibility temperature.

E. H-T phase variation with structural disorder in epitaxial films

So far, we have measured and discussed two types of characteristic fields associated with two different H-T phase boundaries: (1) a vortex solid glass and a vortex liquid separated by a sharp $H_{irr}(T)$, and (2) a phase with vortices individually pinned and one with vortex-vortex interactions divided by the accommodation line $H_{acc}(T)$. The above scenario is illustrated in Fig. 11 based on the fitting lines of our experimental results. The accommodation line is buried deeply within the vortex glass region. It has been proposed to call the vortex state below $H_{acc}(T)$ a strong glass, so as to emphasise the strongly pinned vortex solid and particularly individual pinning in such a state. Above that, the vortex state is formed in the collective pinning regime, which may be viewed as a quasilattice or weak glass. The line of $H_{acc}(T)$ is displayed as the strong individual pinning contributed by intrinsic planar structure and other correlated structure disorders. The latter are either linear defects[3-6] (e.g., natural edge and screw dislocations and artificial columnar defects induced by heavy ion irradiation) or planar d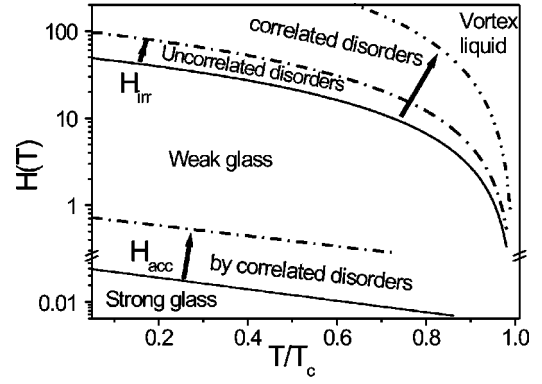efects such as twins and stacking faults.[7,32] These strong pinning sources can effectively increase $H_{acc}(T)$ as well as the IRL. In contrast, uncorrelated disorders such as pointlike defects due to oxygen deficiencies and stress field centres induced by defects or lattice misfits, hardly contribute to H_{acc}. However, they are able to give rise to the enhancement of J_c and the IRL in collective behavior, as evidenced by the present work. We believe that the comprehension of the H-T phase variation with various structure disorders in thin film systems is significant to the development of coated conductors which is established on the technology of epitaxial thin films.

IV. CONCLUSIONS

We have studied the transport and flux pinning properties in high-quality ternary light rare earth GEN123 thin films. Two characteristic fields, the irreversibility field (H_{irr}) and the accommodation field (H_{acc}), are experimentally identified in such a complex thin film system. The irreversibility line, determined by the resistance-temperature transition with a zero-resistance criterion, shows the upward shift to the regime of higher temperatures and fields, compared with pure 123 films. The accommodation field is obtained by the field dependence of transport J_c on a log-log plot which is characterized by a plateau at low fields, and subsequent linear segments at higher fields. In contrast to the improved $H_{irr}(T)$ and J_c, H_{acc} shows no increase arising from the rare earth mixture. For the first time, to our knowledge, we report that H_{acc} vs. T scales as an exponential relation over large range of temperature, and strong enhancement in H_{acc} occurs as the applied field direction varies from $H \| c$ to $H \| (a,b)$. The temperature dependence of J_c is analyzed on the basis of models of thermally activated flux motion and collective flux pinning. It is suggested that the flux pinning mechanism in mixed rare earth films is dominated by stress field centers, which may be locally induced by dislocations and enhanced by lattice mismatch in GEN123 films. According to the fits of experimental $H_{irr}(T)$ and $H_{acc}(T)$, we illustrated the variation of the H-T phases in 123 films, with respect to two sorts of flux pinning sources: correlated and uncorrelated structure disorders. The intrinsic layer structures imply the most pronounced enhancement in both H_{irr}

and H_{acc} when the applied field direction is parallel to the (a, b) plane. We hope that the above analysis provides a quantified guideline for exploring the potential improvement of flux pinning and associated J_c in 123-type thin films as well as coated conductors.

[1] T. L. Hylton and M. R. Beasley, Phys. Rev. B **41**, 11669 (1990).

[2] Ch. Gerber, D. Anselmetti, J. G. Bdenorz, J. Mannhart, and D. G. Schlomm, Nature (London) **350**, 279 (1991).

[3] B. Dam, J. M. Huijbregtse, F. C. Klaassen, R. C. F. van der Geest, G. Doornbos, J. H. Rector, A. M. Testa, S. Freisem, J. C. Martinez, B. Stäuble-Pümpin, and R. Griessen, Nature (London) **399**, 439 (1999).

[4] B. Holzapfel, G. Kreiselmeyer, M. Kraus, G. Saemann-Ischenko, S. Bouffard, S. Klaumünzer, and L. Schultz, Phys. Rev. B **48**, 600 (1993).

[5] L. Krusin-Elbaum, L. Civale, J. R. Thompson, and C. Feild, Phys. Rev. B **53**, 11744 (1996).

[6] D. R. Nelson and V. M. Vinokur, Phys. Rev. B **48**, 13060 (1993).

[7] V. M. Pan and A. V. Pan, Low Temp. Phys. **27**, 732 (2001).

[8] Yu. V. Fedotov, S. M. Ryabchenko, E. A. Pashitskii, A. V. Semenov, V. I. Vakaryuk, V. M. Pan, and V. S. Flis, Low Temp. Phys. **28**, 172 (2002).

[9] H. H. Wen, Z. X. Zhao, R. L. Wang, H. C. Li, and B. Yin, Physica C **262**, 81 (1996).

[10] A. Radhika Davi, V. Seshu Bai, P. V. Patanjali, R. Pinto, N. Harish Kumar, and S. K. Malik, Supercond. Sci. Technol. **13**, 935 (2000).

[11] G. Blatter, M. V. Feigel'man, V. B. Geshkenbein, A. I. Larkin, and V. M. Vinokur, Rev. Mod. Phys. **66**, 1125 (1994).

[12] R. Griessen, Hai-hu Wen, A. J. J. Van Dalen, B. Dam, J. Rector, H. G. Schnack, S. Libbrecht, E. Osquiguil, and Y. Bruynseraede, Phys. Rev. Lett. **72**, 1910 (1994).

[13] H. H. Wen, Z. X. Zhao, Y. G. Xiao, B. Yin, and J. W. Li, Physica C **251**, 371 (1995).

[14] S. Jin, T. H. Tiefel, G. W. Kammlott, R. A. Fastnacht, and J. E. Graener, Physica C **173**, 75 (1991).

[15] Y. Li, N. Chen, and Z. Zhao, Physica C **224**, 391 (1994).

[16] M. Muralidhar, N. Sakai, M. Nishiyama, M. Jirsa, T. Machi, and M. Murakami, Appl. Phys. Lett. **82**, 943 (2003).

[17] M. Muralidhar, N. Sakai, N. Chikumoto, M. Jirsa, T. Machi, M. Nishiyama, Y. Wu, and M. Murakami, Phys. Rev. Lett. **89**, 237001 (2002).

[18] L. Fernández, B. Holzapfel, F. Schindler, B. de Boer, A. Attenberger, J. Hänisch, and L. Schultz, Phys. Rev. B **67**, 052503 (2003).

[19] B. Holzapfel, B. Roas, L. Schultz, P. Bauer, and G. Saemann-Ischenko, Appl. Phys. Lett. **61**, 3178 (1992).

[20] H. Lütgemeier, S. Schmenn, P. Meuffels, O. Storz, R. Schöllhorn, Ch. Niedermayer, I. Heinmaa, and Yu. Baikov, Physica C **267**, 191 (1996).

[21] C. Cai, M. Tachiki, T. Fujii, T. Kobayashi, H. K. Liu, and S. X. Dou, Physica C **356**, 205 (2001).

[22] H. H. Wen and Z. X. Zhao, Phys. Rev. B **50**, 13853 (1994).

[23] M. Tinkham, *Introduction to Superconductivity* (McGraw-Hill, New York, 1996).

[24] M. V. Feigel'man and V. M. Vinokur, Phys. Rev. B **41**, 8986 (1990); M. V. Feigel'man, V. B. Geshkenbein, A. I. Larkin, and V. M. Vinokur, Phys. Rev. Lett. **63**, 2303 (1989).

[25] M. P. Maley, J. O. Willis, H. Lessure, and M. E. McHenry, Phys. Rev. B **42**, 2639 (1990).

[26] E. Mezzetti, R. Gerbaldo, G. Ghigo, L. Gozzelino, B. Minetti, C. Camerlingo, A. Monaco, G. Cuttone, and A. Rovelli, Phys. Rev. B **60**, 7623 (1999).

[27] J. W. Ekin, H. R. Hart, Jr., and A. R. Gaddipati, J. Appl. Phys. **68**, 2285 (1990).

[28] L. Civale, Supercond. Sci. Technol. **10**, A11 (1997).

[29] W. W. Webb, Phys. Rev. Lett. **11**, 191 (1963).

[30] I. A Ovid'ko, J. Phys.: Condens. Matter **13**, L97 (2001).

[31] M. F. Chisholm and S. J. Pennycook, Nature (London) **351**, 47 (1991).

[32] A. Gurevich and L. D. Cooley, Phys. Rev. B **50**, 13563 (1994).